Wide-angle polarization independent infrared broadband absorbers based on metallic multi-sized disk arrays

Cheng-Wen Cheng,[1,2,3] Mohammed Nadhim Abbas,[2] Chao-Wei Chiu,[2] Kun-Ting Lai,[2,4] Min-Hsiung Shih,[2,*] and Yia-Chung Chang[2]

[1]*Department of Physics, National Taiwan University, Taipei 10617, Taiwan*
[2]*Research Center for Applied Sciences, Academia Sinica, Taipei 11529, Taiwan*
[3]*Nano Science and Technology Program, Taiwan International Graduate Program, Academia Sinica, Taipei 11529, Taiwan*
[4]*Institute of Imaging and Biomedical Photonics, National Chiao Tung University, Tainan 71150, Taiwan*
[*]*mhshih@gate.sinica.edu.tw*

Abstract: Two-dimensional metallic broadband absorbers on a SiO_2/Ag/Si substrate were experimentally studied. The absorptivity of such structure can be increased by tailoring the ratio of disk size to the unit cell area. The metallic disk exhibits a localized surface plasmon polariton (LSPP) mode for both TE and TM polarizations. A broadband thermal emitter can be realized because the LSPP mode is independent of the periodicities. By manipulating the ratios and disk sizes, a high-performance, wide-angle, polarization-independent dual band absorber was experimentally achieved. The results demonstrated a substantial flexibility in absorber designs for applications in thermal photovoltaics, sensors, and camouflage.

OCIS codes: (250.5403) Plasmonics; (240.6680) Surface plasmons; (260.3060) Infrared; (160.3918) Metamaterials.

References and links

1. K. B. Alici and E. Ozbay, "Photonic metamaterial absorber designs for infrared solar cell applications," Proc. SPIE **7772**, 77721B (2011).
2. V. E. Ferry, J. N. Munday, and H. A. Atwater, "Design considerations for plasmonic photovoltaics," Adv. Mater. **22**(43), 4794–4808 (2010).
3. K. Nakayama, K. Tanabe, and H. A. Atwater, "Plasmonic nanoparticle enhanced light absorption in GaAs solar cells," Appl. Phys. Lett. **93**(12), 121904 (2008).
4. X. Hu, M. Li, Z. Ye, W. Y. Leung, K.-M. Ho, and S.-Y. Lin, "Design of midinfrared photodetectors enhanced by resonant cavities with subwavelength metallic gratings," Appl. Phys. Lett. **93**(24), 241108 (2008).
5. N. Liu, M. Mesch, T. Weiss, M. Hentschel, and H. Giessen, "Infrared perfect absorber and its application as plasmonic sensor," Nano Lett. **10**(7), 2342–2348 (2010).
6. C.-Y. Tsai, S.-P. Lu, J.-W. Lin, and P.-T. Lee, "High sensitivity plasmonic index sensor using slablike gold nanoring arrays," Appl. Phys. Lett. **98**(15), 153108 (2011).
7. E. Cubukcu, S. Zhang, Y.-S. Park, G. Bartal, and X. Zhang, "Split ring resonator sensors for infrared detection of single molecular monolayers," Appl. Phys. Lett. **95**(4), 043113 (2009).
8. Y.-T. Chang, Y.-C. Lai, C.-T. Li, C.-K. Chen, and T.-J. Yen, "A multi-functional plasmonic biosensor," Opt. Express **18**(9), 9561–9569 (2010).
9. F. J. Rodríguez-Fortuño, M. Martínez-Marco, B. Tomás-Navarro, R. Ortuño, J. Martí, A. Martínez, and P. J. Rodríguez-Cantó, "Highly-sensitive chemical detection in the infrared regime using plasmonic gold nanocrosses," Appl. Phys. Lett. **98**(13), 133118 (2011).
10. A. Unger, U. Rietzler, R. Berger, and M. Kreiter, "Sensitivity of crescent-shaped metal nanoparticles to attachment of dielectric colloids," Nano Lett. **9**(6), 2311–2315 (2009).
11. A. V. Kabashin, P. Evans, S. Pastkovsky, W. Hendren, G. A. Wurtz, R. Atkinson, R. Pollard, V. A. Podolskiy, and A. V. Zayats, "Plasmonic nanorod metamaterials for biosensing," Nat. Mater. **8**(11), 867–871 (2009).
12. W. Kubo and S. Fujikawa, "Au double nanopillars with nanogap for plasmonic sensor," Nano Lett. **11**(1), 8–15 (2011).
13. C. M. Wang, Y. C. Chang, M. W. Tsai, Y. H. Ye, C. Y. Chen, Y. W. Jiang, S. C. Lee, and D. P. Tsai, "Angular independent infrared filter assisted by localized surface plasmon polariton," IEEE Photon. Technol. Lett. **20**(13), 1103–1105 (2008).

#164113 - $15.00 USD Received 5 Mar 2012; revised 17 Apr 2012; accepted 17 Apr 2012; published 20 Apr 2012

14. C.-W. Cheng, M. N. Abbas, Z.-C. Chang, M. H. Shih, C. M. Wang, M. C. Wu, and Y.-C. Chang, "Angle-independent plasmonic infrared band-stop reflective filter based on the Ag/SiO_2/Ag T-shaped array," Opt. Lett. **36**(8), 1440–1442 (2011).
15. Z. H. Jiang, S. Yun, F. Toor, D. H. Werner, and T. S. Mayer, "Conformal dual-band near-perfectly absorbing mid-infrared metamaterial coating," ACS Nano **5**(6), 4641–4647 (2011).
16. R. Siegel and J. Howell, *Thermal Radiation Heat Transfer* (Hemisphere Publishing Corporation, New York, 1981).
17. P.-E. Chang, Y.-W. Jiang, H.-H. Chen, Y.-T. Chang, Y.-T. Wu, L. D.-C. Tzuang, Y.-H. Ye, and S.-C. Lee, "Wavelength selective plasmonic thermal emitter by polarization utilizing Fabry-Pérot type resonances," Appl. Phys. Lett. **98**(7), 073111 (2011).
18. M. Diem, T. Koschny, and C. M. Soukoulis, "Wide-angle perfect absorber/thermal emitter in the terahertz regime," Phys. Rev. B **79**(3), 033101 (2009).
19. X. Liu, T. Tyler, T. Starr, A. F. Starr, N. M. Jokerst, and W. J. Padilla, "Taming the blackbody with infrared metamaterials as selective thermal emitters," Phys. Rev. Lett. **107**(4), 045901 (2011).
20. M. N. Abbas, C.-W. Cheng, Y.-C. Chang, M.-H. Shih, H.-H. Chen, and S.-C. Lee, "Angle and polarization independent narrow-band thermal emitter made of metallic disk on SiO2," Appl. Phys. Lett. **98**(12), 121116 (2011).
21. T. J. Coutts, "A review of progress in thermophotovoltaic generation of electricity," Renew. Sustain. Energy Rev. **3**(2-3), 77–184 (1999).
22. M. Laroche, R. Carminati, and J.-J. Greffet, "Near-field thermophotovoltaic energy conversion," J. Appl. Phys. **100**(6), 063704 (2006).
23. C. Wu, B. Neuner III, G. Shvets, J. John, A. Milder, B. Zollars, and S. Savoy, "Large-area wide-angle spectrally selective plasmonic absorber," Phys. Rev. B **84**(7), 075102 (2011).
24. J. Hao, J. Wang, X. Liu, W. J. Padilla, L. Zhou, and M. Qiu, "High performance optical absorber based on a plasmonic metamaterial," Phys. Rev. Lett. **96**, 251104 (2010).
25. K. B. Alici, A. B. Turhan, C. M. Soukoulis, and E. Ozbay, "Optically thin composite resonant absorber at the near-infrared band: a polarization independent and spectrally broadband configuration," Opt. Express **19**(15), 14260–14267 (2011).
26. M. G. Moharam, E. B. Grann, D. A. Pommet, and T. K. Gaylord, "Formulation for stable and efficient implementation of the rigorous coupled-wave analysis of binary gratings," J. Opt. Soc. Am. A **12**(5), 1068–1076 (1995).
27. E. D. Palik, *Handbook of Optical Constants of Solids* (Academic, Boston, 1985).
28. R. Gordon, "Light in a subwavelength slit in a metal: propagation and reflection," Phys. Rev. B **73**(15), 153405 (2006).
29. D. F. Swinehart, "The beer-lambert law," J. Chem. Educ. **39**(7), 333–335 (1962).
30. V. E. Ferry, L. A. Sweatlock, D. Pacifici, and H. A. Atwater, "Plasmonic nanostructure design for efficient light coupling into solar cells," Nano Lett. **8**(12), 4391–4397 (2008).

1. Introduction

Localized surface plasmon polaritons (LSPPs) are electromagnetic excitations localized at the metal/dielectric interface with a strong field enhancement and a decay of evanescent wave intensity away from the boundary. One of the important applications of LSPPs is in plasmonic absorbers with a large absorption from the field enhancement near the interface. The absorbers have recently attracted considerable interest in the research for applications such as solar cells [1–3], sensors [4–12], filters [13, 14], and metamaterial coatings [15]. Based on Kirchhoff's law of thermal radiation [16], such absorbers operating in the mid-infrared regime can be used as thermal emitters. The emitters are crucial to several relevant applications, especially in thermal selective mid-infrared (MIR) sources [17–20] and thermalphotovoltaic (TPV) converters [21, 22]. The resonance condition of absorbers sensitively depends on the sizes and geometries. The optical properties of the geometric shapes have been explored, such as strips [4, 18, 23], disks [5, 17, 20, 23, 24] rings [6], split rings [7, 8, 25] crosses [9, 19] crescents [10] and rods [11, 12]. However, most of high-performance absorbers do not have large incident angle tolerance, such as H-shaped [15] and U-shaped structures [25]. In this study, a round-shaped metal disk absorber is applied because it can provide an angle and polarization independent LSPP band over a broad range of incidence angles of up to nearly 90° [5, 20]. The experimental results and numerical simulations performed by using rigorous coupled-wave analysis (RCWA) clearly revealed that the resonant wavelength of the LSPP band is independent of the disk periodicity. Since its highly localized behavior, we also combined six distinct disks in one unit cell to form a broadband absorber with a bandwidth of 2000 nm operating at MIR wavelengths, which can potentially be used as a broadband thermal emitter. We also first experimentally found that the absorptivity of the round-shaped

#164113 - $15.00 USD Received 5 Mar 2012; revised 17 Apr 2012; accepted 17 Apr 2012; published 20 Apr 2012

disk absorber obeying the Beer Lambert law can be enhanced by increasing the ratio of disk size to the unit cell area. By modifying the area filling ratio, we can demonstrate a high-performance, wide-angle, polarization-independent dual band absorber with two maximal absorptivity peaks greater than 84% over a wide range of incident angles.

2. Design and simulation

Figure 1(a) illustrates the geometry of the metallic disk (MD) array structure. An array (with period Λ) of MDs with diameter D and thickness t_{Ag} is deposited on the top and a silver ground plane is on the bottom separated by a thin SiO_2 layer with a thickness t_{SiO2}. The bottom layer acts as a mirror to reflect incident light and block light transmittance. The fabrication of the structure began with e-gun deposition of a 5nm Cr adhesion layer and a 100 nm sliver layer on the top of a silicon (Si) substrate, followed by a thickness of SiO_2 thin film deposited by plasma-enhanced chemical vapor deposition (PECVD). A polymethyl methacrylate (PMMA) layer as an e-beam resist was then spin-coated on the top of the SiO_2 thin-film layer. An array of the round-shaped disks periodically spaced with a lattice constant Λ in x and y directions was defined on the PMMA resist by electron beam lithography (EBL). After developing the resist, a 100-nm-thick sliver layer was deposited. Then, a PMMA lift-off process was carried out by rinsing the sample in acetone for a few minutes and cleaning it with isopropyl alcohol and de-ionized water, respectively. Finally, the completed structure was dried with nitrogen gas. The size of the array structure was 200μm × 200μm. Figure 1(b) shows a scanning electron microscopy (SEM) image of a fabricated specimen with the dimensions of Λ = 1.5 μm, D = 1 μm, t_{Ag} = 100 nm, and t_{SiO2} = 80 nm. To understand the resonant behavior of the structure, its reflectance spectra and resonant mode profiles were simulated by RCWA algorithm [26], where the frequency-dependent complex dielectric constants of silver (Ag) and SiO_2 were obtained from [27].

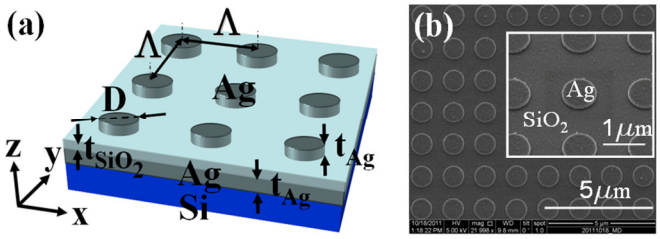

Fig. 1. (a) Schematic diagram of the investigated MD structure. (b) SEM image of a fabricated MD structure. The inset shows the details of the structure within one unit cell at a 35° angle of view.

Figures 2(a) and 2(b) show the TM and TE polarized reflectance spectra of the structure with photon energy ranging from 0.12 eV to 0.64 eV, and the angle of incidence θ_i varying from 0° to 90°. As shown in both TM and TE polarized reflectance spectra, a clear angle-independent resonance absorption band occurs at 0.35 eV, corresponding to a LSPP mode. The mode is caused by a strong coupling between the surface plasmon polariton (SPP) modes of the top MD and bottom silver layers. This strong coupling forms a Fabry–Pérot-like resonance in the SiO_2 cavity as shown in our previous study (see Fig. 2(c) and 2(d) of [20].). According to calculated mode profiles, 72% of $|H_y|^2$ is localized in the SiO_2 layer, and only 28% of $|H_y|^2$ is distributed within the metal region. Because the $|H_y|^2$ distributions are mostly localized within the SiO_2 cavity and less coupling occurred between neighboring MDs, the resonant wavelength is independent of its periodicity; however it is sensitive to individual MD size and the effective index of the medium in the cavity. When the SiO_2 spacer thickness is decreased, the light becomes more concentrated in the resonant cavity and is red-shifted due to increase of the effective index of the mode in the resonant cavity [28]. The RCWA simulation results in the study were also verified by applying 3-D finite-element method (FEM) for the same structure.

#164113 - $15.00 USD Received 5 Mar 2012; revised 17 Apr 2012; accepted 17 Apr 2012; published 20 Apr 2012

Because the resonance is immune to the MD period, it is feasible for applications in broadband emitters and absorbers consisting of various sublattices with various MD resonators corresponding to various absorption bands. According to Kirchhoff's law of thermal radiation, the emittance normalized by the blackbody emittance must be equal to absorptivity at equilibrium. The equality has been demonstrated and reported [19]. If no transmission occurs, the thermal emission spectrum can be predicted by the product of the blackbody radiation profile and the absorptivity integrated over a solid angle

$$Emission(\lambda,T) = B(\lambda,T)\int(1-R(\lambda,\theta,\phi))\cos\theta d\Omega \qquad (1)$$

where B(λ,T) denotes the thermal radiation spectrum of a perfect blackbody (with unit W/m^2) at temperature T, and $1-R(\lambda,\theta,\varphi)$ is the absorptivity of the designed sample. Therefore, through the equation, the thermal emission peaks of the sample can be enhanced by the increased absorptivity at specified resonant wavelengths and temperature. The absorptivity or absorbance is particularly governed by an absorbing species of cross-sectional area and species concentration, which is the well-known Beer Lambert law [29]. The absorptivity or emissivity of the absorber can be improved by modifying the absorption cross section and concentration.

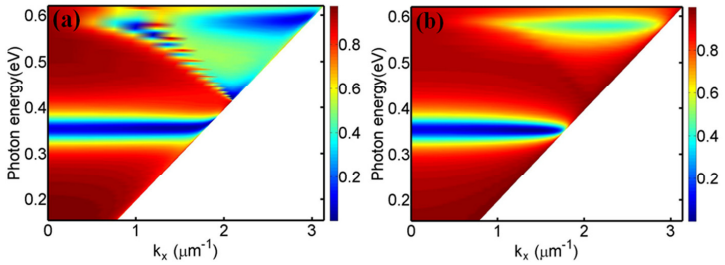

Fig. 2. (a) TM- and (b) TE- mode stimulated reflectance spectra of the MD structure with D = 1 μm, Λ = 1.5 μm, t_{Ag} = 100 nm, and t_{SiO2} = 80 nm.

3. Experimental results and discussion

To characterize the resonant mode and absorptivity A(λ) = 1 - R(λ) of the structure, the reflectivities R(λ) at normal incidence normalized with respect to a bare Ag/Si substrate were measured by using a Fourier transform infrared (FTIR) spectrometer. We also confirmed that the measured absorptivities of the absorbers are nearly the same by using an Ag/Si layer or an Au standard, and the difference between absorptivities from two substrates is less than 3%. A MIR unpolarized light source was focused the sample and reflected back. The back-reflected light through a 50μm × 50μm slit was collected and detected using a MCT (mercury-cadmium-telluride) photodetector with a spectral resolution of 2 cm^{-1}. Figure 3(a) shows the measured resonant wavelengths of the SiO_2 cavities with varying disk sizes when t_{SiO2} = 80 nm and Λ = 1.5 μm. The resonant wavelength is linearly proportional to the MD size (black open squares), in accordance with our simulation (blue solid line). The wavelength tuning rate is approximately 2.8 nm per nm change in D. The absorptivities of the MD arrays versus density and size were also examined. Figure 3(b) displays the absorptivities of the 1 μm MD absorbers with Λ = 1.5, 2, 2.5, 3, 4, and 6 μm. All of the absorption peaks were observed at 3.63 μm, showing an agreement with our simulation in Fig. 2(a) and 2(b). The peak absorptivity with approximately the same FWHM of 0.28 μm increased from 17% to 94% as we diminished the periodicity of the MD array (i.e., an increase in the MD density). The figure of merit (FOM) of the absorber defined as FOM = AQ [30], where A and Q = λ/Δλ are absorptivity and quality factor. The FOM of the metal disk array can be increase from 2.2 to 12 by reducing the periodicity from 6 μm to 1.5 μm. Figure 3(c) shows the absorptivities of the absorbers versus the considered disk sizes D (ranging from 846 nm to 1.88 μm), when Λ =

#164113 - $15.00 USD Received 5 Mar 2012; revised 17 Apr 2012; accepted 17 Apr 2012; published 20 Apr 2012

3 μm. The absorption peaks for D = 846 nm, 1.06 μm, 1.57 μm, 1.36 μm, 1.65 μm, and 1.88 μm were found at λ = 2.96, 3.67, 4.05, 4.65, 5.36, and 5.91 μm with a maximal absorptivity of 47%, 66%, 75%, 85%, 90%, and 95%, respectively. Other high-order modes for D = 1.65 μm and 1.88 μm at λ = 3.40 μm and 3.81 μm, corresponding to CO_2 and water vapor absorption features in the atmosphere were also visible. When the disk size was increased in proportion to its absorption cross-section, the energy absorbed per unit area due to the Fabry–Pérot-like resonance in the MD resonator increased, resulting in a pronounced increase in the absorptivity. Because the MD density and size are associated with the area-fill factor (F), defined as the ratio of MD size to the unit cell area, the dependence of the absorptivity on the fill factor is shown in Fig. 3(d). The absorptivity is linearly proportional to the fill factor when F< 0.24, and it becomes saturated over 90% of absorption when F≧0.24. Therefore, the result that behaves similarly to the Beer Lambert law when F< 0.24 allows us to control the absorption of the MD configuration.

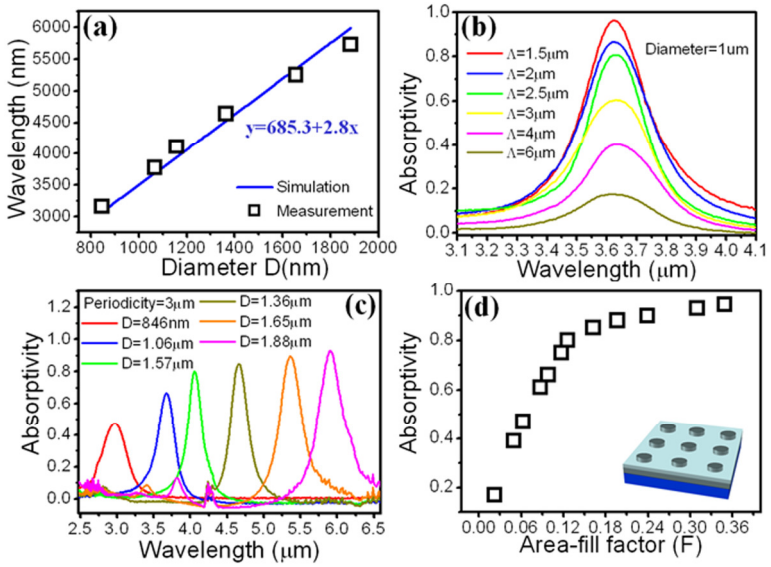

Fig. 3. (a) Comparison of the calculated and measured wavelengths of resonances as functions of the disk diameter D. (b) Absorptivities at normal incidence of the 1 μm MD arrays with several different periodicities Λ. (c) Absorptivities of the MD arrays with different diameters D for Λ fixed at 3 μm. (d) Experimental peak absorptivity of the MD configuration as a function of its area-fill factor F.

With these absorption properties, we present experimental demonstrations of a broadband emitter and a high-performance dual-band absorber. Figure 4(a) shows the absorptivity of the broadband thermal emitter composed of the sublattices with six different disks from 800 nm to 1.35 μm, where the distance between the nearest-neighbor disks is maintained at 1.5 μm. The absorbing spectrum is evidently broad because of the merging of six close peaks located closely to the resonant peaks for each of the single-sized MD absorbers. Although the broadband emitter has a low absorptivity of approximately 35% with a FWHM of 2000 nm centered at the wavelength 4.32 μm, high thermal emittance peaks of the emitter can be achieved by easily increasing heating temperature to modify the thermal dependence of the blackbody emittance curve B(λ,T) as demonstrated in the related literatures [19, 20] without changing emissivity. The purpose the demonstration in Fig. 4(a) is to illustrate that the metal disk array can function as a narrow or broadband absorber as required. Multi-sized disks within one unit cell and large area-fill factors for each of the disks are essential to obtain a broadband absorber with higher absorptivity. However, if all of the disks are patterned on the same layer, a design trade-off occurs between the multi-sized disks and fill factors corresponding to a number of absorption bands and absorption intensities. Despite the trade-

#164113 - $15.00 USD Received 5 Mar 2012; revised 17 Apr 2012; accepted 17 Apr 2012; published 20 Apr 2012

off, a high performance angle and polarization independent dual-band absorber can be realized. Figure 4(b) shows the absorptivity of the dual-band absorber with a SiO_2 spacer of 80 nm where the incident angle varies from 0° and 15°. The two molecule-like disks, D = 825 nm and 960 nm, are arranged to form a 1.5 μm face-centered unit cell with the area-fill factors F = 0.24 and 0.32. The two strong absorption bands at 2.99 μm and 3.40 μm have a maximal absorptivity of 92% and 90% at normal incidence, exhibiting consistency with that predicted by their area-fill factors in Fig. 3(d). The absorptivity in both peaks remains at more than 84% at an oblique incident angle. By effectively modifying the disk sizes and area-fill factors, as well as the SiO_2 spacer thickness, such dual-band absorber configuration can achieve high absorptivity and also offer wide-angle polarization independent flat absorption bands over an angle of incidence of 50° compared with the H-shaped metamaterial coating [15]. It is worth to note that the LSPP mode in each metal disk is highly localized, and independent to periodicity. Therefore the angle-independent absorptivity from the multiple-size disk array is expected, and we also verified it with RCWA simulation.

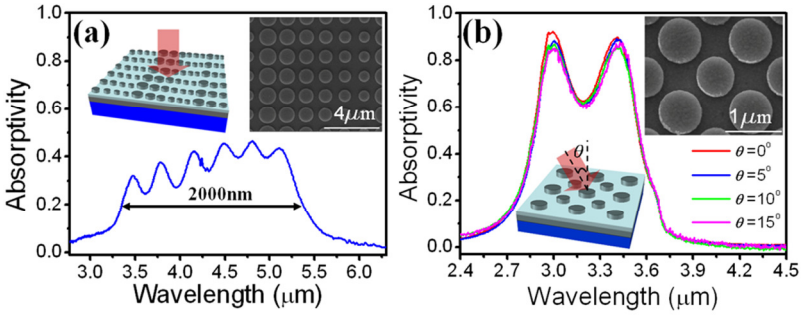

Fig. 4. (a) Experimental absorptivity of the broadband absorber composed of the multi-sized disks with D = 800 nm, 900 nm, 1.03 μm, 1.12 μm, 1.21 μm, and 1.35 μm and a SiO_2 spacer thickness, t_{SiO2} = 32 nm. (b) Absorptivity of the dual-band absorber consisting of two different disk sizes with dimensions D = 825 nm, and 960 nm per unit cell when t_{SiO2} = 80 nm. The insets show the SEM images of one unit cell for the fabricated broadband and dual-band absorbers.

4. Conclusion

In conclusion, we have presented a method to control the absorptivity of the MD absorber by modifying its area-fill factor. Because the LSPP resonances for the MD absorbers are not affected by their array periodicities, a broadband emitter composed of a multi-sized MD array can be realized. An angle and polarization independent dual-band absorber with two maximal absorptivity over 84% can be achieved by controlling the disk sizes and fill factor. The angle of incidence for the absorber can achieve nearly 90° in the operating mid-infrared region from 2.85 μm to 3.65 μm. The approach is applicable for thermal photovoltaic, sensor, and camouflage applications.

Acknowledgment

The authors would like thank the Center for Nano Science & Technology, National Chiao Tung University (NCTU) for the fabrication facilities support. This study is based on research supported by the National Science Council (NSC) of ROC, Taiwan under Grant No. NSC-99-2112-M-001-033-MY3 and by the Grant of the Academia Sinica, Taiwan.

#164113 - $15.00 USD Received 5 Mar 2012; revised 17 Apr 2012; accepted 17 Apr 2012; published 20 Apr 2012